Published in final edited form as:
Vision Res. 2005 December ; 45(28): 3469–3486.

Imaging of nitric oxide in the retina*

William D. Eldred[1] and **Todd A. Blute**
Laboratory of Visual Neurobiology, Department of Biology, Boston University, 5 Cummington Street, Boston, MA 02215, USA

Abstract

Nitric oxide (NO) is the most widespread signaling molecule found in the retina in that it can be made by every retinal cell type. NO is able to influence a wide variety of synaptic mechanisms ranging from increasing or decreasing neurotransmitter release to the modulation of gap junction conductivity. Although biochemical methods can analyze overall levels of NO, such methods cannot indicate the specific cell types involved. In the last few years, fluorescent imaging methods utilizing diaminofluorescein have allowed the real-time visualization of neurochemically or light stimulated NO-induced fluorescence (NO-IF) in specific retinal cells. Recent experiments have shown that this NO-IF can be stabilized using paraformaldehyde fixation. This aldehyde stabilization has allowed the imaging of NO production in the dark and in response to light, as well as the neurochemical modulation of light stimulated NO production. The results of these studies indicate that NO is not always freely diffusible and that NO is largely retained in many cells which make it. The NO production in retina is highly damped in that in the absence of stimulation, the endogenous levels of NO production are extremely low. Finally, different neurochemical or light stimulation protocols activate NO production in specific cells and subcellular compartments. Therefore, although the NO signaling is widespread in retina, it is very selectively activated and has different functions in specific retinal cell types. The use of NO imaging will continue to play a critical role in future studies of the function of NO in retina and other neural systems.

Keywords

Retina; Nitric oxide; Imaging; cGMP; Signal transduction

1. Introduction

The retina is a massively parallel analog visual processing computer that uses a wide variety of neurotransmitters and millions of synaptic connections. A large percentage of these connections involve conventional neurotransmitter release at anatomically defined synaptic connections onto well characterized and localized receptors to produce postsynaptic changes in electrical activity at the millisecond time scale. However, many of these same transmitters and receptors can also activate biochemical signal transduction systems which process this same information at the millisecond to minutes time scales. In recent years, it has become apparent that the nitric oxide(NO)/cyclic guanosine monophosphate(cGMP)signaling pathway is one of the most wide-spread in the retina(Eldred,2000).This pathway is distinguished by having NO produced on demand, that NO is not released using synaptic vesicles, and that NO does not bind to specific receptors on the post synaptic membrane. Basically, any synaptic mechanism that can increase intracellular calcium either directly through receptor channels or by release from intracellular stores can potentially activate this pathway. This increased

*This research was funded by NIH EY04785 to WDE.

[1]Corresponding author. Tel.: +1 617 353 2439; fax: +1 617 358 1124.E-mail address:eldred@bu.edu (W.D. Eldred).

calcium can activate calmodulin which in turn activates either endothelial nitric oxide synthase (eNOS) or neuronal nitric oxide synthase (nNOS) to synthesize NO.

NO has been shown to influence the physiology of all neuronal types in the retina. The most clearly characterized downstream signaling pathway for NO has been the activation of soluble guanylate cyclase (sGC) to synthesize cGMP. For instance, NO has been shown to increase the gain and extend the voltage range of exocytosis in cone photoreceptors (Rieke & Schwartz, 1994; Savchenko, Barnes, & Kramer, 1997). In bipolar cells, NO donor produces an inward current accompanied by a rise in dim and bright flash response amplitudes, and an increase in membrane conductance (Shiells & Falk, 1992). Cyclic GMP has recently been shown to selectively enhance responses to dim, but not bright, stimuli through a purely postsynaptic mechanism that is blocked by inhibitors of cGMP-dependent kinase (Snellman & Nawy, 2004). These last authors propose that cGMP-dependent kinase decreases coupling of the ON-bipolar cell metabotropic glutamate receptors to their downstream signaling cascade, which has the effect of amplifying small decreases in photoreceptor transmitter release.

Perhaps the most comprehensive studies have examined the role of NO in horizontal cells. Miyachi, Murakami, and Nakaki (1990), report that injection of the NO precursor, L-arginine, into H1 luminosity-type horizontal cells in turtle retina reduces their light responses, dramatically increases their input resistance, decreases their response to a surround, and increases their response to stimulation of their receptive field center.McMahon and Ponomareva (1996) report that bath application of L-arginine also decreases the kainate responses in H1 cells in a manner similar to cGMP and NO. Thus, it is likely that the H1 horizontal cells can serve as their own source and target of NO to negatively modulate the gain at photoreceptor-horizontal cell synapses. Finally, Yu and Eldred (2003) have shown that $GABA_A$ and $GABA_C$ receptor antagonists increase retinal cGMP levels through the activation of nitric oxide synthase (NOS) and that NO stimulates GABA release and inhibits glycine release in retina (Yu & Eldred, 2005). The NO stimulated GABA release from horizontal cells was shown to be due to the reversal of the GABA uptake transporter.

In amacrine cells, Mills and Massey (1995) conclude that by working through cGMP, the NO released by light stimulation (Koistinaho, Swanson, de Vente, & Sagar, 1993) decreases the rod input and increases the cone input during light adaptation by uncoupling the AII amacrine cells from the cone bipolars. Wexler, Stanton, and Nawy (1998) demonstrate that NO can depress $GABA_A$ receptor function on amacrine cells. They conclude that NO stimulates sGC to increase cGMP levels, which then increases phosphorylation through protein kinase G to depress GABA currents. The increased cGMP also stimulates a cGMP-activated phosphodiesterase to decrease cAMP levels and phosphorylation through protein kinase A. Wexler et al. (1998)conclude that activators of adenylate cyclase, like dopamine, enhance $GABA_A$ currents, while activators of guanylate cyclase, like NO, do the opposite, and therefore cAMP and NO/ cGMP function in a push-pull mechanism in GABAergic transmission in these amacrine cells. NO also modulates cyclic nucleotide gated channels by activating a NO-sensitive sGC to increase levels of cGMP in photo-receptors (Savchenko et al., 1997), bipolar cells (Shiells & Falk, 1992), and ganglion cells (Ahmad et al., 1994). Finally, Wang, Liets, and Chalupa (2003) report that bath application of L-arginine or NO donor usually reduces the peak discharge rates of ON responses in ganglion cells by about 40%, and completely blocks the OFF responses in most ganglion cells.

Clearly, the NO/cGMP signaling system is critical for many aspects of retinal function and it will be important to understand its role in specific retinal cell types. In particular, it will be important to analyze which cells contain specific NOS isoforms, what stimuli can activate NO production in identified cells, and what downstream signaling pathways are activated by the NO that is produced. Answers to these questions have been facilitated through the use of

isoform specific nNOS antisera, fluorescent imaging methods to image NO in retina (Blute, Lee, & Eldred, 2000), and the use of antiserum directed against cyclic guanosine monophosphate (cGMP). report will describe the methods used for NO imaging and how they can be combined with the study of specific NOS isoforms and the cGMP signaling systems downstream from NO. It will also provide the light and electron microscopic localizations of nNOS in the retina that are necessary to put the NO imaging in perspective.

2. Methods

2.1. Imaging hardware and software

The images in this report were captured using one of three camera/imaging software packages. The first was an Apogee AP-7 cooled, thinned, back-illuminated CCD camera with 512 × 512 pixel resolution (Apogee Instruments, Auburn, CA) controlled with MaxIm DL CCD imaging software (Cyanogen Productions, Ottawa, Ont.). This camera was attached to an Olympus BH-2 epifluorescence microscope with the normal filters for fluorescein. This camera system has very high sensitivity but a slow frame acquisition rate (one 16 bit frame/10 s). The second and third systems were attached to a conventional Olympus BX-51WI fluorescence microscope with a 75 xenon arc lamp (Oriel lamp housing, Oriel, Irvine, CA; Opti Quip model 1600 power supply, Opti Quip; Highlands Mills, NY). The filters used for NO-IF are an Omega 475 nm ±40 nm excitation filter (XF1073), the appropriate dichroic mirror (XF 2010), and a 515-575 nm bandpass emission filter (XF3010) (Omega Optical Brattleboro, VT). The second system camera was an OlymPix FK1300 cooled CCD camera (Olympus) with 640 × 480 pixel resolution, driven by Merlin imaging software (Life Science Resources) that provided control over the 12-bit TIFF image capture (up to 4 frames per second). Finally, our current system camera is a Hamamatsu Orca II-ER CCD camera (Hamamatsu, K.K., Japan) with 1344 × 1024 pixel resolution controlled by UltraView software (Perkin-Elmer, Boston, MA) (Perkin-Elmer). The exact camera specifications in terms of sensitivity, integration time, and bit depth are not overly critical because the NO-IF signal is quite strong. Any imaging setup which can be used to image fluorescein isothiocyanate fluorescence can be used to image NO-induced fluorescence (NO-IF).

2.2. Tissue preparation, stimulation, fixation, and NO imaging

Larval tiger salamanders (Ambystoma tigrinum) or adult turtles (Pseudemys scripta elegans) were maintained on 12 h light/12 h dark cycles. These animals were decapitated near the middle of the light phase of their light-dark cycle, using a method approved by the Boston University Charles River Campus Institutional Animal Care and Use Committee, and their eyes were quickly removed and hemisected. For light microscopy, the isolated eyecups were fixed in 4% paraformaldehyde in 0.1 M phosphate buffer (PB, pH 7.4) for 60-90 min and then processed as previously described (Blute, Mayer, & Eldred, 1997) to produce 14 μm thick cross-sections on slides. For electron microscopy, the isolated eyecups were processed as previously described using a sequential low pH-high pH paraformaldehyde fixation protocol (Eldred, Zucker, Karten, & Yazulla, 1983). After fixation, the retinas were cryoprotected using a graded sucrose/glycerol buffer series before being frozen and then sectioned using a sliding microtome with a freezing stage into 70 μm thick tangential sections.

Animals used for NO imaging were dark adapted overnight and were maintained in total darkness by using infrared imaging equipment throughout the preparation, dye loading, and pharmacological stimulation treatments of the retinal slices. Retinal slices were prepared as described previously (Lukasiewicz, Maple, & Werblin, 1994). Briefly, the eyes were enucleated and the anterior portion of the eye and lens were removed, the eyecup was hemisected, placed vitreous side down on nitrocellulose filters, and sectioned into 250 μm thick slices. Slices were allowed to recover from slicing for at least 30 min and then incubated for

60 min in Ringer solution (110 mM NaCl, 2.5 mM KCl, 3 mM $CaCl_2$,2 mM $MgCl_2$, 10 mM glucose, and 5 mM Hepes, pH 7.6) containing 10 μM of the NO-sensitive dye 4-amino-5-methylamino-2',7'-difluorofluorescein diacetate (DAF) (Molecular Probes, Eugene, Oregon) with or without the following: 1 mM L-arginine, or the NOS inhibitors 100 μM N-nitro-monomethyl-L-arginine (LNMMA), 100 μM 7-nitroindazole (7-NI), or 100 μM S-methyl-L-thiocitrulline (SMTC). The slices were washed for 45 min with fresh aerated Ringer and then placed into light tight boxes that were fitted with a fiber optic attachment. Some slices were stimulated for 10 min with a light emitting diode to produce either flashing (660 nm, 3 Hz, 20 μW, 25% duty cycle) or steady light (660 nm, 20 μW) stimulation, while a matched set of slices were kept in the dark for comparison. In other cases, after loading with DAF the slices were pharmacologically stimulated in room light with the following drugs: the NO donor (±)-S-nitroso-N-acetylpenicillamine (SNAP, 100 μM), bicuculline (10- 100 μM), picrotoxin (10-100 μM), or nicotine (50 μM).

In some cases, the NO-IF was observed real-time using a conventional fluorescence microscope equipped with excitation and emission filters normally used to view fluorescein. In the kinetic studies presented here the fluorescent images were captured of the NO-IF in the slices using an OlymPix FK1300 cooled CCD camera driven by Merlin imaging software. The data was plotted using the Origin graphing package (Northhampton, MA). In other cases, following light or pharmacological stimulation the slices were then fixed in the dark for 2 h with 4% paraformaldehyde in 0.1 M phosphate buffer (PB, pH 7.4) and then washed in PB. The NO-IF was then imaged using an Olympus Fluoview 300 confocal microscope and its associated Fluoview software. The images of NO-IF are presented in reverse contrast such that the NO-IF is dark. In some cases the three-dimensional rendering software on a Zeiss LSM510NLO two-photon confocal microscope was used to analyze the confocal stacks obtained from the Olympus confocal microscope.

2.3. Neuronal NOS immunocytochemistry

The same reagents and general methods were used for both the light and electron immunocytochemistry. The cryostat sections were processed on the slides. The non-specific binding was eliminated by blocking the sections using a combination of 10% normal goat serum and an avidin/biotin-blocking kit (Vector Laboratories, Burlingame, CA). For the light microscopy, we employed two different rabbit primary neuronal NOS (nNOS) antisera that were each used at a dilution of 1:5000. The first was directed against rat nNOS (SC-648, Santa Cruz Biotechnology, Santa Cruz, CA), while the second was raised against porcine cerebellar nNOS (Mayer, Mathias, & Bőhme, 1990). The retinal sections were then processed using Vector Elite ABC reagents (Vector Laboratories, Burlington, CA) diluted 1:1000 and Immunopure Metal Enhanced DAB substrate (Pierce Chemical, Rockford, IL). For confocal microscopy the nNOS primary antisera were localized using 1:500 goat anti-rabbit Alexa 568 secondary antiserum (Molecular Probes). There was no labeling in unlabeled control tissues when the primary antiserum was omitted, or when the primary antiserum was preincubated with the peptide fragments against which the primary antiserum were raised.

2.4. Neuronal NOS electron microscopy

The 70-μm thick tangential sections for electron microscopy were processed as free-floating sections using the SC-648 nNOS antiserum. We chose to use the nNOS antiserum from Santa Cruz because it was less negatively influenced by the fixation required for electron microscopy. After several rinses in PB, the immunostained tangential sections were flattened and post-fixed in 1% osmium in PB for 90 min. Following several rinses in PB, the sections were dehydrated using an acetone series and embedded in Medcast Araldite 502 resin (Ted Pella, Redding, CA) between plastic sheets. Areas of interest were cut from the flattened retinas and re-embedded to allow cutting of cross-sections. The thin sections were examined without heavy metal

counterstain using a Philips 410 electron microscope. The subsequent negatives were digitally scanned using a flat-bed scanner and the figures were arranged and labeled using Corel Draw 11 software (Corel, Ottawa, Ontario, Canada).

2.5. Cyclic GMP immunocytochemistry

All antisera solutions were diluted in PB with 0.3% Triton X-100 (PBtx). Following imaging of NO-IF, some slices were incubated in 1.5% normal goat serum for 60 min, and then for three days in a rabbit-derived primary antiserum (used at 1:500) directed against cGMP (de Vente, Steinbusch, & Schipper, 1987). Following several washes in PB, the slices were incubated in 1:500 goat anti-rabbit Alexa 568 (Molecular Probes). Incubation of this same cGMP antiserum with free cGMP has been previously shown to eliminate all staining (Blute, Velasco, & Eldred, 1998). The cGMP-LI was then imaged using an Olympus Fluoview 300 confocal microscope and its associated Fluoview software.

2.6. Comparison of real-time and paraformaldehyde fixed NO-IF

Imaging NO using DAF requires the use of bright light sources to view the increased NO-IF in the presence of NO. This would normally preclude the use of DAF to image NO production in the dark. Previous studies have shown that aldehydes can be used to stabilize activated DAF in tissues (Kasim, Branton, & Clarke, 2001; Sugimoto, Fujii, Takemasa, & Yamashita, 2000). We reasoned that we could use aldehyde fixation to stabilize the activated DAF to visualize the NO-IF produced in the dark using conventional confocal microscopy. However, this DAF fixation protocol has not been applied previously to examine retinal slices. To validate our method, we performed control fixation experiments to show that the fixation did not non-specifically increase NO-IF and that fixation did not alter the localization of NO-IF. For these experiments, we prepared salamander retinal slices and loaded them with DAF as described above. To simplify these experiments, the retinas were stimulated with 50 μM nicotine in Ringer for 10 min. Immediately, following this pharmacological stimulation, fluorescent images were captured of the NO-IF in the slices using a Hamamatsu Orca ER CCD camera attached to an Olympus BW50WI microscope equipped with epifluorescence illumination. Following this initial imaging, the Ringer covering the slices was replaced with 4% paraformaldehyde in PB. Subsequent fluorescent images were obtained of the same slices while still in fixative after 30 min.

2.7. NO-selective electrode measurements

Measurement of the levels of NO near individual retinal neurons were made using the Mark II ISO-NO NO meter in combination with an ISO-NOPNM NanoSensor NO-selective probe which is reported to have a tip diameter of 0.1 μm and a detection limit for NO of less than 0.5 nM (World Precision Instruments, Sarasota, FL). The probe was held using a micromanipulator and the tip was visually placed near the cell to be measured. Before each experiment, the meter and probe combination were calibrated using a standard curve of known concentrations of NO. The calibration was done using decomposition of a S-nitrosothiol compound using Cu (I) as a catalyst (www.wpiinc.com, World Precision Instruments). The output of the NO meter was recorded through a Cambridge Electronics Designs (Cambridge, UK) Micro 1401 A/D computer interface running their Spike 2 electrophysiology software.

3. Results

Both the light and electron microscopic localizations of nNOS-LI in the turtle retina have been reported previously in detail (Blute et al., 1997; Cao & Eldred, 2001; Haverkamp & Eldred, 1998), but they will be briefly reviewed here to allow the subsequent NO imaging to be put into perspective.

3.1. Light microscopic localization of nNOS

In these studies we used an older lot of Santa Cruz nNOS (SC-648) primary antiserum for the immunocytochemical staining. Unfortunately, the presently available lot of this same antiserum does not produce this same high quality staining. When we used our lot of the SC-648 antiserum in turtle it was possible to clearly distinguish three distinct amacrine cell types with nNOS-like immunoreactivity (nNOS-LI, Figs. 1A-C). The type 1 nNOS amacrine cells (Fig. 1A) were relatively common and in retinal cross-sections they had large vertically oriented darkly staining pyriform shaped somata with relatively symmetric dendritic arborizations. Their processes in the deeper portions of the inner plexiform layer (IPL) were studded with boutons. The type 2 amacrine cells (Fig. 1B) were the most common of the three nNOS amacrine cell types in the turtle retina. These cells had smallish, moderately stained, rounded somata that gave rise to several delicate processes, which ran a short distance in the outer IPL, before branching extensively in the central IPL and giving rise to terminal processes deep in the IPL or among the somata in the ganglion cell layer (GCL). Finally, the type 3 amacrine cells (Fig. 1C) had large, flattened, oval somata that often gave rise to thick, faintly labeled primary processes that arborized in the outer IPL. The type 1 and 2 amacrine cell types in turtle were very similar to the ND1 and ND2 (Vaney & Young, 1988) or type 1 and type 2 (Sagar, 1990) NADPH-diaphorase positive amacrine cell types in the rabbit, and to the NDa and NDb NADPH-diaphorase positive amacrine cell types in the guinea pig (Cobcroft, Vaccaro, & Mitrofanis, 1989).

In contrast, when the primary antiserum directed against porcine cerebellar nNOS (Mayer et al., 1990) was used there was much more extensive labeling. With this antiserum there was nNOS-LI in photoreceptor ellipsoids, many amacrine cell somata, near the outer limiting membrane, in many boutons and processes in the IPL, and in numerous somata in the GCL (Fig. 1D). It is possible that the differences in labeling seen with these two antisera indicate that they may be recognizing alternate expressions of nNOS such as the natural variants of nNOS produced in the central nervous system by selective alternative splicing of the nNOS gene (Iwasaki et al., 1999).

3.2. Ultrastructural localization of nNOS-LI

No significant labeling was seen in the bipolar or horizontal cell somata at the ultrastructural level, although patches of nNOS-LI have been associated with horizontal cell membranes in the OPL and there is nNOS-LI in the tips of some bipolar and horizontal cell processes that are postsynaptic to photoreceptor ribbon synapses and at basal junctions between photoreceptors (Haverkamp & Eldred, 1998). The lack of stronger somatic labeling in horizontal and bipolar cells at the ultrastructural level is probably due to the decreased antigenicity caused by the fixation protocol used for electron versus light microscopy.

Neuronal NOS-LI was found associated with the outer membranes of the nucleus and the endoplasmic reticulum, and as diffuse flocculent immunoreactivity in the cytoplasm in some amacrine cell somata (Fig. 2A). In the IPL many amacrine cell processes had strong nNOS-LI. These processes could be identified as amacrine cell processes by their lack of synaptic ribbons and the presence of synaptic vesicles at conventional synapses. In some labeled amacrine cells, the electron-dense reaction product diffusely filled the entire cell process (Fig. 2B).

Neuronal NOS-LI was also present in the ellipsoid in the inner segments of rods (not shown) or the accessory elements of the double cones (Fig. 3A') in some atypical mitochondria that were interspersed among the conventional mitochondria composing the ellipsoid. These atypical mitochondria were characterized by having poorly developed cristae. The adjacent conventional mitochondria in the ellipsoid showed no such increases in electron density. In

some presumptive amacrine cell processes, there were also conventional mitochondria with nNO-SLI in their intermembrane space (Fig. 3B′). These labeled mitochondria were distinct from those in the photoreceptor ellipsoids, in that in the photoreceptors there was granular immunoreactivity in the matrix and they had poorly developed cristae. In contrast, the labeled mitochondria in the amacrine cell profiles had nNOS-LI which was more selectively confined to the intermembrane space and they had well defined cristae.

In some amacrine cell boutons in the IPL, the nNOSLI was selectively associated with the presynaptic specializations (Fig. 3C′), with relatively little cytoplasmic nNOS-LI. Some amacrine cells made more than one conventional synaptic contact in a given bouton, only some of which had nNOS-LI at their presynaptic specialization (Fig. 3C′). It was likely that this nNOS-LI was truly presynaptic because in more weakly labeled preparations, it was possible to clearly see the nNOSLI was associated with clusters of synaptic vesicles and that there were the conventional parallel membrane specializations.

Selective subcellular localization of nNOS-LI was also seen in some bipolar cell axon terminals (Fig. 3D′). In these bipolar terminals, the immunoreactivity was present in a small cytoplasmic region associated with the plasma membrane a micron or less from the ribbon synapse. In this specialized region, the two plasma membranes ran parallel to one another forming a uniform extracellular space. Although the parallel membranes and the consistent extracellular space suggested the existence of a synapse, the density of the nNOS-LI in this region obscured any clusters of synaptic vesicles.

At the ultrastructural level, very few somata in the GCL contained nNOS-LI and the labeling was much weaker than found in amacrine cell somata. Most of the nNOS-LI was associated with the endoplasmic reticulum or was located diffusely in the cytoplasm. The existence of nNOS-LI in some axons in the ganglion cell axon layer supported that some of these labeled somata were ganglion cells. Neuronal NOS-LI was present in mitochondria in Müller cells near the outer limiting membrane and in patches in Müller processes in the IPL. There was also some nNOS-LI associated with Müller cell villi surrounding the photoreceptors.

3.3. Nitric oxide imaging

The selective localization of nNOS-LI at specific synapses or in select mitochondria seems at odds with it being a freely diffusible gas which has been suggested to potentially diffuse 100s of microns (Wood & Garthwaite, 1994). Furthermore, although the NOS immunocytochemistry suggested that there were a wide variety of potential sources for NO production, questions remained as to which sources were active under what circumstances and how the NO spread in retina.

Kojima et al. (1998a,1998b) developed the NO specific fluorescent probe diaminofluorescein (DAF). When DAF is nitrosated by reactive nitrogen oxides such as N_2O_3 at one of its amino groups the reaction leads to the formation of the triazole DAF-2T. DAF is relatively non-fluorescent until it binds the NO oxidation product and forms DAF-2T which increases the quantum efficiency of its fluorescence by ~180-fold (Kojima et al., 1998b). When this dye is used to label retinal slices, it is possible to localize NO production within specific retinal cell types.

3.4. Specificity controls for imaging NO

In cell-free solutions, the fluorescence increase produced by the combination of DAF and NO donor shows a linear relationship between the concentration of NO donor in the solution and the rate of increase of NO (Blute et al., 2000; Nagata, Momose, & Ishida, 1999). This occurs because in a cell-free solution, the NO donor is continuously liberating NO. Thus, the increase

in NO-IF over time represents an integral of the NO production. These results suggested that the rate of increase in fluorescence can be correlated with the relative concentration of NO.

In slices loaded with DAF and illuminated with 490 nm light, there was a slight fluorescence throughout the unstimulated control retinas which allowed the visualization of some labeled somata and the plexiform layers (Fig. 4A). These weakly labeled somata are probably a reflection of the endogenous levels of NO in control tissue. When illuminated over time, there was a small steady decrease in this baseline fluorescence probably due to bleaching (Fig. 4B). This indicates that the light stimulation itself does not activate DAF. The addition of the NO-donor, SNAP, caused an immediate overall increase in fluorescence throughout the slice which confirmed that all of the cells were loaded with DAF and that there was no obvious subcellular compartmentalization of the DAF (Fig. 4C). Addition of depleted SNAP resulted in no such change in fluorescence.

All NMDA-stimulated increases in fluorescence were eliminated by inhibiting NOS. Slices that were pre-incubated and imaged in the presence of the potent irreversible NOS inhibitor, 100 μM L-NMMA, exhibited no increases in fluorescence in response to 250 μM NMDA (Figs. 5A and B). This control is consistent with the fluorescence being due to the production of NO by NOS. Adding exogenous arginine to the loading Ringer enhanced the increase in fluorescence in response to NMDA stimulation, but did not evoke an increase in NO-IF by itself or alter the cell types responding to NMDA. A similar arginine-stimulated enhancement of DAF fluorescence is reported in several previous studies (Kojima et al., 1998a; Nakatsubo et al., 1998).

In total, these control experiments confirmed that the increased fluorescence we saw in response to NMDA stimulation was correlated with increased NO production resulting from NMDA receptor activation. With the results of these controls in mind, we use the term NO-IF.

3.5. Anatomical localization of NO production

In the turtle retina, at the light microscopic level, nNOS-LI is present in three amacrine cell types and their processes in the IPL, in ganglion cell somata, in photoreceptor inner segments, and in Müller cell processes near the outer limiting membrane (Blute et al., 1997). Moreover, detailed ultrastructural investigations find nNOS-LI in photoreceptors, horizontal cells, and bipolar cells in the outer retina (Cao & Eldred, 2001; Haverkamp & Eldred, 1998). NMDA stimulation is able to increase NO-IF in all of these locations in select cells throughout the retina (Blute et al., 2000). This NMDA-stimulated increase in NO production is consistent with the previous results of Blute et al. (1998) showing that NMDA can increase levels of cGMP by activating NOS in turtle retina.

All of the images in Fig. 6 were captured real-time from live slices of turtle retina. In some but not all photoreceptors, NMDA-stimulated NO-IF increased throughout the entire inner segment, soma and synaptic terminal (Fig. 6A). The increased NO-IF was first observed in the ellipsoid, and the strongest overall increases in NO-IF in photoreceptors were in the ellipsoid. Within 30 s, lower levels of increased NO-IF were seen in photoreceptor somata and synaptic terminals. The presence of oil droplets indicated that at least some of these photoreceptors were cones. The high levels of NO-IF seen in the ellipsoid, agree with the immunocytochemical and histochemical localization of NOS in this region (Blute et al., 1997;Cao & Eldred, 2001;Koch, Lambrecht, Haberecht, Redburn, & Schmidt, 1994)in many species. It is likely that the NO-IF seen in photo receptors seen response to NMDA may relate to the NMDA receptor subunits that have been previously localized presynaptically within both rod and cone photoreceptor terminals (Fletcher, Hack, Brandstatter, & Waässle, 2000).

The previous ultrastructural localization of nNOS-LI at specific contacts in the OPL (Haverkamp & Eldred, 1998) is consistent with the strong NMDA-stimulated increase in NO-IF seen in the OPL. Horizontal (Fig. 6B) and bipolar cell (Fig. 6C) somata with NOIF were observed only occasionally, but fluorescent processes in the OPL were common (Figs. 6B and C). Previous physiological studies support NO production by horizontal cells in the turtle retina (Miyachi et al., 1990) and in the hybrid bass retina (McMahon & Ponomareva,1996).Although NMDA receptors have not been localized on turtle horizontal or bipolar cells, it is possible that the NMDA stimulated NO-IF in these cells may also relate to the NMDA receptors localized on both rod and cone photoreceptor terminals (Fletcher et al., 2000). If NMDA activates these receptors to increase glutamate release from photoreceptors, this glutamate could activate the kainate receptors which have been shown to activate bipolar and horizontal cells (Marc, 1999).

A prominent feature of retinal nNOS-LI would be the numerous labeled amacrine cell somata (Blute et al., 1997). Consistent with the strong nNOS-LI observed in multiple amacrine cell types, NMDA dramatically increased NO-IF in a wide variety of amacrine cells (Figs.6D-G). Amacrine cells stimulated with NMDA exhibited several different forms of NO-IF. Many amacrine cells had increased NO-IF that was confined to their somata (not shown), while in other cases the NO-IF increased in both their somata and processes (Figs. 6D-G). Some of the labeled amacrine cells had swellings on their processes that resembled synaptic boutons (Fig. 6E), while others did not (Figs. 6F and G). When present, the active boutons often had more intense NOIF than the rest of the adjacent process, although the NO-IF in boutons was still often weaker than seen in the somata of the same cells. There were also activated processes in the IPL that were not directly associated with labeled somata (Fig. 6I). These isolated processes with NO-IF usually had boutons. In addition, there were isolated boutons with high NO-IF found in the IPL that were not associated with any labeled processes (Fig. 6D).

Immunocytochemistry indicates that there is nNOS confined within many somata in the GCL in turtle (Blute et al., 1997). In response to NMDA, some somata in the GCL exhibited some of the strongest increases in NO-IF seen in the retina (Figs. 6D, G, and I). Interestingly, although the NO-IF appeared to diffuse out of these somata in the GCL, it did not fill the processes of these cells as it did in many of the adjacent amacrine cells.

Previous studies have described the presence of nNOS in Müller cells, although they usually have much less nNOS-LI than other retinal cell types (Kurenni et al., 1995; Liepe, Stone, Koistinaho, & Copenhagen, 1994). In turtle, there is little apparent nNOS-LI in Müller cells (Blute et al., 1997). Considerable NO-IF appeared in Müller cells after several minutes of NMDA stimulation. These increases in NO-IF in Müller cells would often begin in their processes near the outer or inner limiting membranes and spread centrally to their soma (Fig. 6H). In the GCL and ganglion cell axon layer (GCAL), Müller cell end feet had small varicosities (less than 5 μm in diameter) with strong NO-IF (Fig. 6J). It is likely that the NMDA stimulated increases in NO-IF in Müller cells may relate to the NMDA receptors which have been shown to be present on Müller cells in human retina (Puro, Yuan, & Sucher, 1996) and the nNOS-LI which has been reported in Müller cells in turtle retina (Cao & Eldred, 2001).

In conclusion, every retinal cell type, but not every cell of a given type can show increases in NO-IF. It is interesting that all of the cells of a specific anatomical type, i.e., H1 horizontal cells, do not show a uniform response in that only some show increased NO-IF in response to a given stimulus. This raises the possibility that there may be neurochemical differences between anatomically similar retinal cells in that only some may utilize the NO/cGMP signaling pathway. This idea of selective localization is supported by the localization of nNOS-LI in only some rod bipolar cell dendrites in rat retina (Haverkamp & Eldred, 1998).

These NO imaging results confirmed previous light and electron microscopic immunocytochemical studies (Blute et al., 1997; Cao & Eldred, 2001; Haverkamp & Eldred, 1998; Liepe et al., 1994) which demonstrated NOS in every cell type in the retina and at specific synaptic contacts.

3.6. Kinetics of NO-IF production in response to blocking GABAergic inhibition or stimulation with NMDA

In response to pharmacological stimulation, somatic increases in NO-IF all followed a similar general time-course, when intensity levels were plotted against time (Fig. 7). During the rising phase, the intensity of NOIF increased exponentially from baseline levels to a transient peak, which was immediately followed by a slower exponential decrease. For each of these pharmacological stimuli the different sources of NO-IF had characteristic time-courses. Though some ganglion cells differed in their peak responses, their response kinetics were similar. The same kinetic similarities were seen for other sources such as amacrine cell somata or boutons. Interestingly, ganglion cells showed a more sharply peaked response to 100 μM NMDA, while the boutons showed a more sharply peaked response to picrotoxin/bicuculline. However, amacrine cell somata had less steep rising and falling phases than did ganglion cells. Boutons in the IPL displayed less stereotypic responses and more variability, with a slower, more linear (less exponential) rising phase, a lower relative peak, and often a slower decay. In some cases, the increases in NO-IF in some boutons and ganglion cells had shorter onset latency in response to blockade of GABAergic inhibition than those seen in response to NMDA.

3.7. Quantification of the apparent diffusion of NO-IF

In some cells, the NO-IF spread well beyond their cell boundaries (Figs. 6G and I), as would be predicted by the previous models of NO diffusion (Wood & Garthwaite, 1994). However, in many cells, even in cells with very high levels of NO-IF, there was relatively little spread of NO-IF beyond the cell boundary (Fig. 6E) and the NOIF did not spread more than 10 μm from the source. In contrast, in some other cells, particularly somata in the GCL, there was considerable spread beyond the site of production (Figs. 6G and I). These differences in spread were often seen between two different cell types within the same retinal slice, which would support there being a cell specific control over the spread of NO.

It is possible to use small NO-selective electrodes to measure the NO levels near a single retinal neuron.Fig. 8A shows the NO-electrode placed near a soma in the GCL, while Fig. 8B shows the change in the concentration of NO in response to stimulation with 100 μM NMDA. In this case the NO concentration rose from the preexisting background concentration of ~96 to ~174 nM which indicates that DAF is able to easily detect changes in nanomolar levels of NO. Given that there may be some retention of NO within the soma, it is possible that the intracellular levels of NO were higher than 174 nM. Such quantitative measurements of NO levels can then be used to quantify the NO levels within a given digital image because there is a linear relationship between the NO concentration and NO-IF (Blute et al., 2000). Surprisingly, even if an intracellular NO concentration of 174 nM is assumed, there are NO concentrations below 10 nM within 10-20 lm away from relatively strong sources of NO production. This further supports a rather limited spread of NO in some cases.

3.8. Aldehyde fixation of DAF

Previous studies have shown that aldehydes can be used to stabilize activated DAF in tissues (Kasim et al., 2001; Sugimoto et al., 2000). We reasoned that aldehyde fixation could stabilize the activated DAF to visualize NO produced in the dark using conventional confocal microscopy. However, this DAF fixation protocol has not been applied previously to examine retinal slices. To validate this method, control fixation experiments were performed to show

that the fixation did not non-specifically increase NO-IF and that fixation did not alter the localization of NO-IF.

One particular advantage of this method is that if the DAF is activated before it is fixed with paraformaldehyde, it will remain activated after fixation. Fig. 9A shows the NO-IF in a living turtle retinal slice that has been stimulated with 20 μM picrotoxin. The NO-IF was present in what appears to a bipolar cell terminal. Fig. 9B shows a comparable slice that was also stimulated with picrotoxin before being fixed with paraformaldehyde. The labeling in this fixed slice closely resembled that seen in the live slice. The fixation also provided several other beneficial results. There was an apparent increase in NO-IF in response to aldehyde fixation as has been described previously (Sugimoto et al., 2000). This increase in NO-IF was often so substantial as to require a decrease in the gain of the CCD camera to successfully capture the image. The fixation and subsequent increase in NO-IF also made it much easier to use confocal microscopy to obtain high resolution images. Finally, fixation seems to optically clear the tissue which makes it easier to obtain confocal images from deeper portions of thick retinal slices. Fig. 10 shows a three dimensional rendering of NO-IF in a retinal slice that was stimulated with 660 nm flashing light before being fixed with aldehydes.

To confirm that fixation did not non-specifically increase NO-IF and that fixation did not alter the localization of NO-IF, retinal slices were stimulated with 50 μM nicotine and then imaged before and following fixation. In Fig. 11 the red color indicates the NO-IF that was present following 10 min of stimulation before fixation. The green color indicates the NO-IF that was present following 30 min of paraformaldehyde fixation. The yellow color indicates the NO-IF that was present before and after fixation. There is virtually no pure green in the image indicating that fixation did not induce or create any NO-IF that was not there prior to fixation. There is however extensive red over the photoreceptors which indicates that much of the NO-IF in the photoreceptors was lost during fixation. It is possible that photoreceptors lack some binding element that paraformaldehyde can cross-link with DAF to retain activated DAF within the photoreceptors. The increased NO-IF in horizontal cells may be related to the uncoupling effects of cholinergic agonists that have been reported in horizontal cells in mudpuppy retina (Myhr & McReynolds, 1996). Thus there is no indication that fixation produces any artifactual production of NOIF or DAF activation and that in some cell types there can be a decrease in NO-IF in response to fixation. This aldehyde fixation method is thus ideal for studying light stimulated NO production in retina.

3.9. Light stimulated NO-IF

The ability to use paraformaldehyde fixation to stabilize NO-IF allows the analysis of NO production in the dark and in response to various light stimulation protocols. It is also possible to use a multi-photon confocal microscope to image NO-IF real-time using an 810-nm excitation wavelength without activating or bleaching the photoreceptors (Eldred, personal communication). However, this method is expensive and logistically challenging. It is much simpler to use aldehyde fixed DAF. If the dark adapted retinal slices are made in the dark using infrared imaging equipment, then loaded with DAF and washed in the dark, it is possible to image the levels of NO-IF that are present in the dark. In salamander retina in the dark, there was strong NO-IF in many horizontal cells, some somata in the INL, and some photoreceptors (Fig. 12A'). As described above, there may be a potential loss of NO-IF from photoreceptors so this photoreceptor labeling may be underrepresented. We examined the light-driven NO-IF in dark adapted retinal slices. In steady light, there was still NO-IF in some photoreceptors and horizontal cells, but there were also some somata in the GCL, many more somata in the INL, and many boutons in the IPL with strong NO-IF (Fig. 12B'). In flashing light there was still strong NO-IF in the same sources seen with steady light, but there was much stronger NO-IF in more amacrine cell somata, in somata in the GCL, and in processes and numerous boutons

in the IPL (Fig. 12C'). These results indicate that NO is part of a light activated signaling pathway.

It is interesting that the production of NO-IF in horizontal cells is increased by light in that photoreceptor transmitter release is reduced in the light which should hyperpolarize the horizontal cells. This result suggests that activation of NOS is not purely by influx of extracellular calcium and that other sources of calcium may be involved. For instance, it is possible that metabotropic receptors, such as the mGluR5 receptors reported to be present on horizontal cells (Hartveit, Brandstatter, Enz, & Wassle, 1995) may be activating release of calcium from intracellular stores to increase NO-IF. It is also important to point out that the dark adapted retinas had been dark adapted for several hours and the increased levels of NO-IF may be a reflection of this long adaptation time. The levels of NO-IF were highest in flashing light, versus steady light or darkness, which indicates the transition between light to dark may be the strongest activator of NO production.

3.10. Colocalization of nNOS-LI with NO-IF

The ability to fix NO-IF with paraformaldehyde allows imaging of NO-IF to be combined with conventional nNOS immunocytochemistry. This can serve as a control to confirm that increases in NO-IF are due to the activation of NOS; and by using isoform specific NOS antisera it is possible to associate these increases with particular isoforms of NOS. Moreover, it is possible to determine which of a population of NOS containing cells can be selectively activated by a particular stimulus.

Fig. 13 shows NO-IF in retinal slices that have been stimulated with 50 μM nicotine and then immunocytochemically labeled using an antiserum directed against nNOS. In these images the NO-IF is green, the nNOSLI is red, and the yellow indicates that it was nNOS that was producing the NO-IF. Interestingly, the yellow double labeling indicated that nicotine primarily activated nNOS in the somata of amacrine cells and in not their processes in the IPL. In contrast, nicotine increased levels of NO-IF in both the somata and some primary processes in horizontal cells (Fig. 13B). Finally, these images indicate that nicotine did not activate the nNOS in all of the cells that contained it (red somata in Fig. 13A) and further that nicotine increased NO-IF in cells which did not contain nNOS-LI (green somata in Fig. 13B). This suggests that another NOS isoform, perhaps eNOS was also activated by nicotine.

3.11. Imaging NO-IF and the downstream production of cGMP

The use of paraformaldehyde fixation also allows the simultaneous visualization of the cells which produce NO-IF and the cells in which soluble guanylate cyclase is activated to produce the synthesis of cGMP. When retinal slices were stimulated with 50 μM nicotine and imaged using a combination of NO-IF and cGMP immunocytochemistry, it was evident that in turtle retina some horizontal cells can have primarily have NO-IF alone (Fig. 14, green somata with horizontal arrow), while other horizontal cells can show an increase in NO-IF and also show a cell autonomous increase in cGMP-LI (Fig. 14, vertical arrowheads). These results indicate that the entire NO/cGMP signaling pathway can be functionally demonstrated using a combination of imaging of NO-IF and cGMP immunocytochemistry.

4. Discussion

4.1. Correlation of the localization of nNOS-LI and NO-IF

The light and electron microscopic localization of nNOS-LI indicated that every cell type in the retina had nNOS-LI. Furthermore, in many of these cells the localization was surprisingly specific in that the nNOSLI was found at specific synapses or it was associated with certain cellular organelles. This relative specificity is seemingly at odds with the suggestions that NO

can diffuse for 100s of microns (Wood & Garthwaite, 1994). The imaging of NO-IF strongly supports the broad immunocytochemical localization of nNOS-LI in that it was possible to see NO-IF in every location where there was nNOS-LI. In addition, the selective localization of nNOS-LI was also reflected in the specificity of NO-IF, in that the NO-IF could be seen within photoreceptor ellipsoids or individual synaptic boutons. This close anatomical correlation also confirms that NO-IF truly represents NO being synthesized by NOS. However, the fact that some of the NO-IF does not colocalize with nNOS-LI suggests that other NOS isoforms, most likely eNOS are also involved. Additional double labeling studies of eNOS-LI and NO-IF should clarify this issue.

4.2. Diffusion of NO from specific cellular sources

Previous reports (Wood & Garthwaite, 1994) have suggested that NO is freely diffusible. However, the present imaging of NO-IF would suggest that this is not always the case. It appeared that for many sources there was relatively little diffusion, while for other sources there was considerable diffusion. There were also differences in the extent of intracellular diffusion. For instance, in some amacrine cells the NO-IF completely filled the cell, including its processes, with little extracellular diffusion. It is likely that these results indicate that NO can spread much less from some sources than others. Since all of the cells contain DAF, if the NO diffuses out of one cell it will activate the DAF in the contiguous cells (Figs. 6G and I) and thus be detected. The fact that both apparent diffusion and lack of diffusion was seen in different cells in the same slice (Fig. 6G) would strongly support that a lack of diffusion was not an artifact of the DAF imaging method.

NO-IF does not support free diffusion models of NO signaling. It is also possible to functionally show a lack of spread of NO in retina. When a retina is stimulated with a NO donor it is possible to activate all of the sGC to synthesize cGMP (Blute et al., 1998). If NO was freely diffusible then the pattern of cGMP production should resemble that seen with a broadly applied NO donor. This was not the case however. For example, stimulation with nicotine strongly activated NO and cGMP production in horizontal cells (Fig. 13), but no increases in cGMP were seen in closely adjacent bipolar and amacrine cells which have been shown to contain NO activatible sGC in previous studies (Blute et al., 1998). Clearly, the NO does not diffuse the few microns from the horizontal cells to the adjacent bipolar and amacrine cells containing sGC.

There was also relatively little spread of NO-IF out from individual boutons, although it is likely there would still be enough spread to move the 1-3 lm from one synapse to an adjacent bouton. It is interesting to note that the NO-IF in some boutons did not appear to spread through the cell processes interconnecting them. In contrast, many somata in the GCL showed considerable spread of NO-IF. However, even in the case of diffusion out of these somata in the GCL, there was no apparent diffusion of NO-IF into the processes of these cells. This suggests that in addition to mechanisms which retain NO within the entire cell, there are also mechanisms to control the movement of NO within a single cell. The fact that DAF has been calculated to have only a~ 9.6% binding efficiency (Nakatsubo et al., 1998) suggests that over 90% of the NO would be free to diffuse as it normally would. This again supports that if NO was spreading, we could image its spread.

There are several possibilities why the NO would not be more freely diffusible. One likely explanation is that the NO is bound to thiols such as glutathione to form nitrosothiols such as glutathione (Hogg, 2002; Singh, Hogg, Joseph, & Kalyanaraman, 1996; Upchurch, Welch, & Loscalzo, 1995). Very high levels of glutathione have been localized in specific retinal cell types such as Müller cells and horizontal cells (Pow & Crook, 1995). Such a functional cellular sink for NO has been suggested to be involved in shaping low level NO signals (Griffiths & Garthwaite, 2001). NO is a non-polar molecule that can selectively partition into the cell membranes. Malinski et al. (1993) used a NO selective porphyrinic sensor to measure the NO

concentrations in different regions of endothelial cells and found significantly higher concentrations of NO within the endothelial cell membrane in comparison to the concentrations in the cytosol. This relatively high concentration of NO in the membrane might prevent diffusion of NO from the cell because the relatively lower levels of NO in the cytoplasm would be blocked from leaving the cell by the high concentrations of NO in the membrane. It is also possible that membrane surface thiols may regulate the cellular entry of NO, which could in turn regulate its exit. Finally, protein disulfide isomerase (PDI) is able to catalyze thio-disulfide exchange reactions to facilitate the transfer of NO from the extracellular to the intracellular compartments (Zai, Rudd, Scribner, & Loscalzo, 1999). Thus enzymes like PDI could serve to transport any NO that leaves the cell, back into the cell using a mechanism involving transnitrosation.

4.3. Methodological considerations

There are a number of reports which have raised various issues in relation to potential difficulties in using DAF to image NO production. Roychowdhury, Luthe, Keilhoff, Wolf, and Horn (2002) report that DAF is more sensitive to peroxynitrite than to NO. This idea is not supported by the present colocalizations of NO-IF and cGMP-LI in the same cells, as it is NO that activates sGC. Their observations perhaps represent a unique situation that occurs in glial cultures, but does not occur in retina. Our results supporting that DAF does react with NO are consistent with the original reports by Kojima et al. (1998a,1998b) who state that DAF does not react with nitrate, nitrite, superoxide, hydrogen peroxide, or peroxynitrite (also Blute, personal communication).

Nagata et al. (1999) report that the reaction of DAF with NO donors in a fluorescence spectrometer is reduced or abolished by catecholamines, ascorbate, and reducing agents like glutathione. They suggest it is likely that these compounds serve to trap the NO and prevent it from reacting with DAF. Endogenous catecholamines are only a problem if you want to image NO production within catecholinergic neurons. More selective synthetic drugs which target catecholamine receptors do not inhibit DAF fluorescence (Nagata et al., 1999).

DAF is reported to react not with NO itself, but with reactive nitrogen oxides such as N_2O_3. Reducing agents such as ascorbate or reduced glutathione can scavenge such reactive nitrogen oxides and thus inhibit the activation of DAF (Nagata et al., 1999). However, a recent report by Rodriguez, Specian, Maloney, Jourdheuil, and Feelisch (2005) has shown that this is not a critical issue in a cellular environment as opposed to a chemical system. DAF is usually applied as a cell permeable diacetate form which is then cleaved by intracellular esterases to form a cell impermeable DAF which remains trapped in the cells. Using quantitative high pressure liquid chromatographic analysis, Rodriguez et al. (2005) estimated the concentration of DAF-related products in the tissue to be~400 μM. They concluded that at these concentrations DAF could successfully compete with these reducing agents for the reactive nitrogen oxides. Even in the presence of these high concentrations of DAF, these authors concluded that NO production and signaling remained unchanged in aortic rings. However, these authors also conclude that although these high intracellular concentrations of DAF can overcome these nitrogen oxide scavengers, these high DAF concentrations can give rise to a background DAF fluorescence which can limit its effective sensitivity and make basal measurements of NO difficult. The difficulty of this background DAF fluorescence can be minimized by using lower concentrations of DAF for loading and by careful choice of the emission filter wavelength used to image the NO-IF. Much of the background DAF fluorescence is below 515 nm, while much of the NOIF of DAF is above this wavelength (Kojima et al., 1998b). Thus, it is much better to use a long pass emission filter with a steep cutoff at 515 nm.

Broillet, Randin, and Chatton (2001) report that DAF is influenced by factors other than NO, such as calcium and the light used to image DAF. However, a subsequent study by Suzuki et

al. (2002) using NO gas itself revealed that the reaction of DAF and NO was completely independent of calcium and magnesium at physiological concentrations. Suzuki et al. (2002) also showed that calcium did not enhance the conversion of DAF into its fluorescent product (DAF triazole), but that it enhanced the release of NO from the NO donor used in the Broillet et al. (2001) study. Although our results did not indicate the activation of DAF by light (Figs. 4 and 5) it is, however, true that bright light can release NO that is bound to intracellular sinks like glutathione (Sexton, Muruganandam, McKenney, & Mutus, 1994), therefore it is best to only illuminate the DAF when images of the NO-IF are being captured.

A number of controls can be used to confirm that the NO-IF being imaged is due to NO being synthesized by NOS. The use of a NOS inhibitor can be used to confirm the enzymatic production of NO as opposed to the release of NO from bound stores (Fig. 5). It is also valuable to try to correlate the changes in NO with a separate indicator of NO production, such as increased cGMP levels (Fig. 14) or by measurements using NO selective electrodes. The involvement of specific isoforms of NOS in the production of NO can be analyzed by colocalizing the increases in NO-IF with immunocytochemically identified specific NOS isoforms (Fig. 13).

5. Conclusions

NO/cGMP is the most widely distributed signaling pathway in the retina in that NO can be selectively produced in every cell type in the retina. The use of NO-IF imaging and functional NO measurements indicate the diffusion of NO can be largely limited with in a single cell or even a single synaptic bouton, or in other cases there can be significant diffusion. The correlation of NO production with cGMP synthesis suggests that NO can function as both an intra- and intercellular signaling molecule. The application of NO imaging has been crucial to establish much of what is currently known about NO in the retina and it will form the basis of many future studies. Although these imaging techniques and methods for analyzing the NO/cGMP signaling pathway have focused on the retina, all of these same methods are broadly applicable to all neural systems.

Acknowledgments

We wish to thank Felicitas B. Eldred for excellent technical assistance, Drs. S. H. Haverkamp and L. Cao for the electron immunocytochemistry, and Dr. Paul B. Cook for his help with the light stimulation experiments. I would like to thank Deborah Whitney for help with preparation of the manuscript. This research was funded by NIH EY04785 to WDE.

References

Ahmad I, Leinders-Zufall T, Kocsis JD, Shepherd GM, Zufall F, Barnstable CJ. Retinal ganglion cells express a cGMP-gated cation conductance activatable by nitric oxide donors. Neuron 1994;12:155–165. [PubMed: 7507337]

Blute TA, Mayer B, Eldred WD. Immunocytochemical and histochemical localization of nitric oxide synthase in the turtle retina. Visual Neuroscience 1997;14:717–729. [PubMed: 9279000]

Blute TA, Velasco P, Eldred WD. Functional localization of soluble guanylate cyclase in turtle retina: Modulation of cGMP by nitric oxide donors. Visual Neuroscience 1998;15:485–498. [PubMed: 9685201]

Blute TA, Lee MR, Eldred WD. Direct imaging of NMDA-stimulated nitric oxide production in the retina. Visual Neuroscience 2000;17:557–566. [PubMed: 11016575]

Broillet M, Randin O, Chatton J. Photoactivation and calcium sensitivity of the fluorescent NO indicator 4,5-diaminofluorescein (DAF-2): Implications for cellular NO imaging. Federation of European Biochemical Societies Letters 2001;491:227–232. [PubMed: 11240132]

Cao L, Eldred WD. Subcellular localization of neuronal nitric oxide synthase in turtle retina: Electron immunocytochemistry. Visual Neuroscience 2001;18:949–960. [PubMed: 12020086]

Cobcroft M, Vaccaro T, Mitrofanis J. Distinct patterns of distribution among NADPH-diaphorase neurones of the guinea pig retina. Neuroscience Letters 1989;103:1–7. [PubMed: 2779850]

de Vente J, Steinbusch HWM, Schipper J. A new approach to immunocytochemistry of 3´,5´-cyclic guanosine mono-phosphate: Preparation specificity and initial application of a new antiserum against formaldehyde-fixed 3´,5´-cyclic guanosine mono-phosphate. Neuroscience 1987;22:361–373. [PubMed: 2819779]

Eldred, WD. Nitric oxide in the retina. In: Steinbusch, HMW.; de Vente, J.; Vincent, S., editors. Handbook of chemical neuroanatomy, functional neuroanatomy of the nitric oxide system. 17. 2000. p. 111-145.

Eldred WD, Zucker C, Karten HJ, Yazulla S. Comparison of fixation and penetration enhancement techniques for use in ultrastructural immunocytochemistry. Journal of Histochemistry and Cytochemistry 1983;31:285–292. [PubMed: 6339606]

Fletcher EL, Hack I, Brandstatter JH, Waässle H. Synaptic localization of NMDA receptor subunits in the rat retina. Journal of Comparative Neurology 2000;420:98–112. [PubMed: 10745222]

Griffiths C, Garthwaite J. The shaping of nitric oxide signals by a cellular sink. Journal of Physiology 2001;536:855–862. [PubMed: 11691877]

Hartveit E, Brandstatter JH, Enz R, Waässle H. Expression of the mRNA of seven metabotropic glutamate receptors (mGluR1 to 7) in the rat retina. An in situ hybridization study on tissue sections and isolated cells. European Journal of Neuroscience 1995;7:1472–1483. [PubMed: 7551173]

Haverkamp SH, Eldred WD. Localization of nNOS in photoreceptor, bipolar and horizontal cells in turtle and rat retinas. NeuroReport 1998;10:2231–2235. [PubMed: 9694205]

Hogg N. The biochemistry and physiology of S-nitrosothiols. Annual Review of Pharmacology and Toxicology 2002;42:585–600.

Iwasaki T, Hori H, Hayashi Y, Nishino T, Tamura K, Oue S, Lizuka T, Ogura T, Esumi H. Characterization of mouse nNOS2, a natural variant of neuronal nitric-oxide synthase produced in the central nervous system by selective alternative splicing. Journal of Biological Chemistry 1999;274:17559–17566. [PubMed: 10364190]

Kasim N, Branton RL, Clarke DJ. Neuronal nitric oxide synthase immunohistochemistry and 4,5-diaminofluorescein diacetate: Tools for nitric oxide research. Journal of Neuroscience Methods 2001;112:1–8. [PubMed: 11640952]

Koch K-W, Lambrecht H-G, Haberecht M, Redburn D, Schmidt HHHW. Functional coupling of a Ca^{2+}/ calmodulin-dependent nitric oxide synthase and a soluble guanylyl cyclase in vertebrate photoreceptor cells. European Molecular Biology Organization Journal 1994;13:3312–3320.

Koistinaho J, Swanson RA, de Vente J, Sagar SM. NADPH-diaphorase (nitric oxide synthase)-reactive amacrine cells of rabbit retina: Putative target cells and stimulation by light. Neuroscience 1993;57:587–597. [PubMed: 7508576]

Kojima H, Nakatsubo N, Kikuchi K, Kawahara S, Kirino Y, Nagoshi H. Detection and imaging of nitric oxide with novel fluorescent indicators: Diaminofluoresceins. Analytical Chemistry 1998a;70:2446–2453. [PubMed: 9666719]

Kojima H, Sakurai K, Kikuchi K, Kawahara S, Kirino Y, Nagoshi H. Development of a fluorescent indicator for nitric oxide based on the fluorescein chromophore. Chemical and Pharmaceutical Bulletin 1998b;46:373–375.

Kurenni DE, Thurlow GA, Turner RW, Moroz LL, Sharkey KA, Barnes S. Nitric oxide synthase in tiger salamander retina. Journal of Comparative Neurology 1995;361:525–536. [PubMed: 8550897]

Liepe BA, Stone C, Koistinaho J, Copenhagen DR. Nitric oxide synthase in Müller cells and neurons of salamander and fish retina. Journal of Neuroscience 1994;14:7641–7654. [PubMed: 7527846]

Lukasiewicz PD, Maple BR, Werblin FS. A novel GABA receptor on bipolar cell terminals in the tiger salamander retina. Journal of Neuroscience 1994;14:1202–1212. [PubMed: 8120620]

Malinski T, Taha Z, Grunfeld S, Patton S, Kapturczak M, Tomboulian P. Diffusion of nitric oxide in the aorta wall monitored in situ by porphyrinic microsensors. Biochemical and Biophysical Research Communications 1993;193:1076–1082. [PubMed: 8323533]

Marc RE. Kainate activation of horizontal, bipolar, amacrine and ganglion cells in the rabbit retina. Journal of Comparative Neurology 1999;407:65–76. [PubMed: 10213188]

Mayer B, Mathias J, Böhme E. Purification of a Ca^{2+}/ calmodulin-dependent nitric oxide synthase from porcine cerebellum. Federation of European Biochemical Societies 1990;277:215–219.

McMahon DG, Ponomareva LV. Nitric oxide and cGMP modulate retinal glutamate receptors. Journal of Neurophysiology 1996;76:2307–2315. [PubMed: 8899605]

Mills SL, Massey SC. Differential properties of two gap junctional pathways made by AII amacrine cells. Nature 1995;377:734–737. [PubMed: 7477263]

Miyachi E, Murakami M, Nakaki T. Arginine blocks gap junctions between retinal horizontal cells. NeuroReport 1990;1:107–110. [PubMed: 2129864]

Myhr KL, McReynolds JS. Cholinergic modulation of dopamine release and horizontal cell coupling in mudpuppy retina. Vision Research 1996;36:3933–3938. [PubMed: 9068846]

Nagata N, Momose K, Ishida Y. Inhibitory effects of catecholamines and anti-oxidants on the fluorescence reaction of 4,5-diaminofluorescein, DAF-2, a novel indicator of nitric oxide. Journal of Biochemistry 1999;125:658–661. [PubMed: 10101276]

Nakatsubo N, Kojima H, Kikuchi K, Nagoshi H, Hirata Y, Maeda D. Direct evidence of nitric oxide production from bovine aortic endothelial cells using new fluorescence indicators: Diaminofluoresceins. Federation of European Biochemical Societies 1998;427:263–266.

Pow DV, Crook DK. Immunocytochemical evidence for the presence of high levels of reduced glutathione in radial glial cells and horizontal cells in the rabbit retina. Neuroscience Letters 1995;193:25–28. [PubMed: 7566658]

Puro DG, Yuan JP, Sucher NJ. Activation of NMDA receptor-channels in human retinal Muller glial cells inhibits inward-rectifying potassium currents. Visual Neuroscience 1996;13:319–326. [PubMed: 8737283]

Rieke F, Schwartz EA. A cGMP-gated current can control exocytosis at cone synapses. Neuron 1994;13:863–873. [PubMed: 7946333]

Roychowdhury S, Luthe A, Keilhoff G, Wolf G, Horn TF. Oxidative stress in glial cultures: Detection by DAF-2 fluorescence used as a tool to measure peroxynitrite rather than nitric oxide. Glia 2002;38 (2):103–114. [PubMed: 11948804]

Rodriguez J, Specian V, Maloney R, Jourd́heuil D, Feelisch M. Performance of diamino fluorophores for the localization of sources and targets of nitric oxide. Free Radical Biology and Medicine 2005;38:356–368. [PubMed: 15629864]

Sagar SM. NADPH-diaphorase reactive neurons of the rabbit retina: Differential sensitivity to excitotoxins and unusual morphologic features. Journal of Comparative Neurology 1990;300:309–319. [PubMed: 2148324]

Savchenko A, Barnes S, Kramer RH. Cyclic-nucleotide-gated channels mediate synaptic feedback by nitric oxide. Nature 1997;390:694–698. [PubMed: 9414163]

Sexton DJ, Muruganandam A, McKenney DJ, Mutus B. Visible light photochemical release of nitric oxide from S-nitrosoglutathione: Potential photochemotherapeutic applications. Photochemistry and Photobiology 1994;59(4):463–467. [PubMed: 8022889]

Shiells RA, Falk G. Retinal on-bipolar cells contain a nitric oxide-sensitive guanylate cyclase. NeuroReport 1992;3:845–848. [PubMed: 1358250]

Singh RJ, Hogg N, Joseph J, Kalyanaraman B. Mechanism of nitric oxide release from S-nitrosothiols. Journal of Biological Chemistry 1996;271:18596–18603. [PubMed: 8702510]

Snellman J, Nawy S. cGMP-dependent kinase regulates response sensitivity of the mouse on bipolar cell. Journal of Neuroscience 2004;24:6621–6628. [PubMed: 15269274]

Sugimoto K, Fujii S, Takemasa T, Yamashita K. Detection of intracellular nitric oxide using a combination of aldehyde fixatives with 4,5-diaminofluorescein diacetate. Histochemistry and Cell Biology 2000;113:341–347. [PubMed: 10883393]

Suzuki N, Kojima H, Urano Y, Kikuchi K, Hirata Y, Nagano T. Orthogonality of calcium concentration and ability of 4,5-diaminofluorescein to detect NO. Journal of Biological Chemistry 2002;277:47–49. [PubMed: 11641405]

Upchurch GR Jr. Welch GN, Loscalzo J. S-nitrosothiols: Chemistry, biochemistry, and biological actions. Advances in Pharmacology 1995;34:343–349. [PubMed: 8562444]

Vaney DI, Young HM. GABA-like immunoreactivity in NADPH-diaphorase amacrine cells of the rabbit retina. Brain Research 1988;474:380–385. [PubMed: 3208139]

Wang GY, Liets LC, Chalupa LM. Nitric oxide differentially modulates ON and OFF responses of retinal ganglion cells. Journal of Neurophysiology 2003;90:1304–1313. [PubMed: 12724368]

Wexler EM, Stanton PK, Nawy S. Nitric oxide depresses $GABA_A$ receptor function via coactivation of cGMP-dependent kinase and phosphodiesterase. Journal of Neuroscience 1998;18:2342–2349. [PubMed: 9502795]

Wood J, Garthwaite J. Models of the diffusional spread of nitric oxide: Implications for neural nitric oxide signalling and its pharmacological properties. Neuropharmacology 1994;33:1235–1244. [PubMed: 7870284]

Yu D, Eldred WD. $GABA_A$ and $GABA_C$ receptor antagonists increase retinal cyclic GMP levels through nitric oxide synthase. Visual Neuroscience 2003;20:627–637. [PubMed: 15088716]

Yu D, Eldred WD. Nitric oxide stimulates GABA release and inhibits glycine release in retina. Journal of Comparative Neurology 2005;483:278–291. [PubMed: 15682393]

Zai A, Rudd MA, Scribner AW, Loscalzo J. Cell-surface protein disulfide isomerase catalyzes transnitrosation and regulates intracellular transfer of nitric oxide. Journal of Clinical Investigation 1999;103(3):393–399. [PubMed: 9927500]

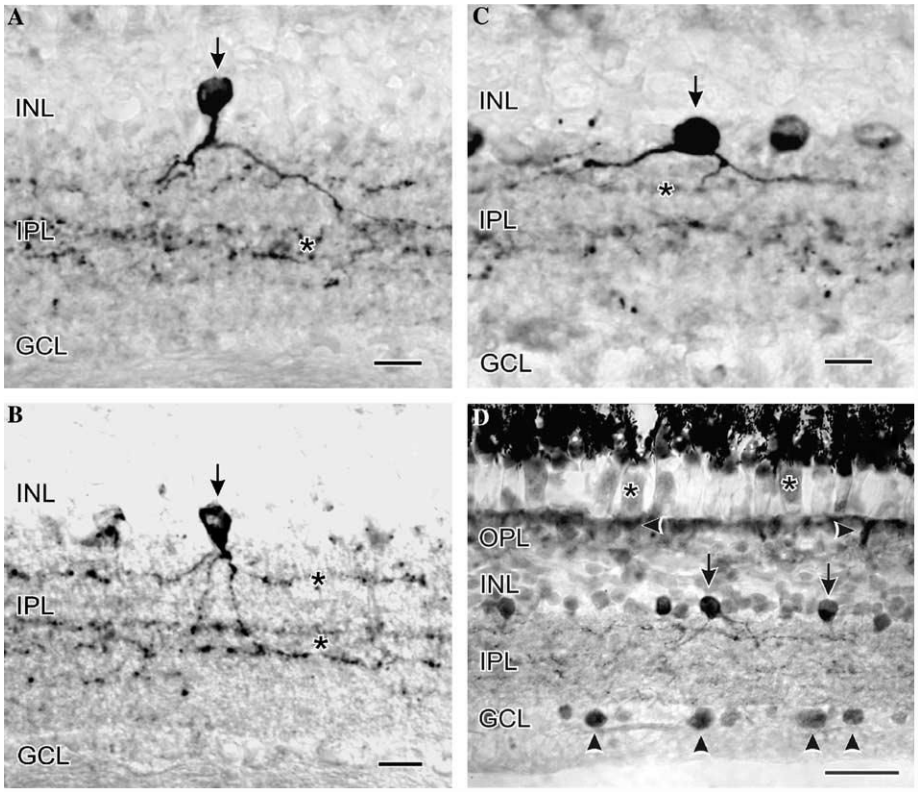

Fig. 1.

At the LM level in turtle retina, strong nNOS-LI was present in at least three amacrine cell types (vertical arrows, type 1 in A; type 2 in B; and type 3 in C), their processes in the IPL (asterisks in A-C), some somata in the GCL (vertical arrowheads in D), the ellipsoids of photoreceptors (asterisks in D) and near the OLM (horizontal arrowheads in D). Some amacrine cell somata had strong nNOS-LI (vertical arrow in D), while numerous amacrine somata had weaker nNOS-LI. The sections in (A-C) were labeled using a rabbit primary antiserum against amino acids 1400-1418 of rat nNOS (SC-648), while the section in (D) was incubated in a rabbit antiserum against porcine cerebellar nNOS (Mayer et al., 1990). Scale bars, A-C, 15 lm; 1D, 30 lm.

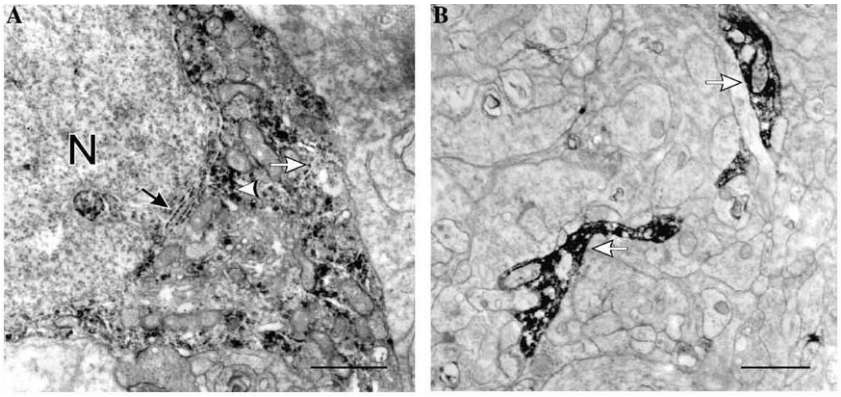

Fig. 2.

(A) In the INL in turtle, nNOS-LI was found associated with the nuclear membrane (black arrow), the endoplasmic reticulum (white arrow), and as diffuse flocculent nNOS-LI (white arrowhead) in the cytoplasm in some amacrine cell somata. (B) In the IPL, electron-dense reaction product diffusely filled some amacrine cell processes (white arrows). Scale bars, 1 lm.

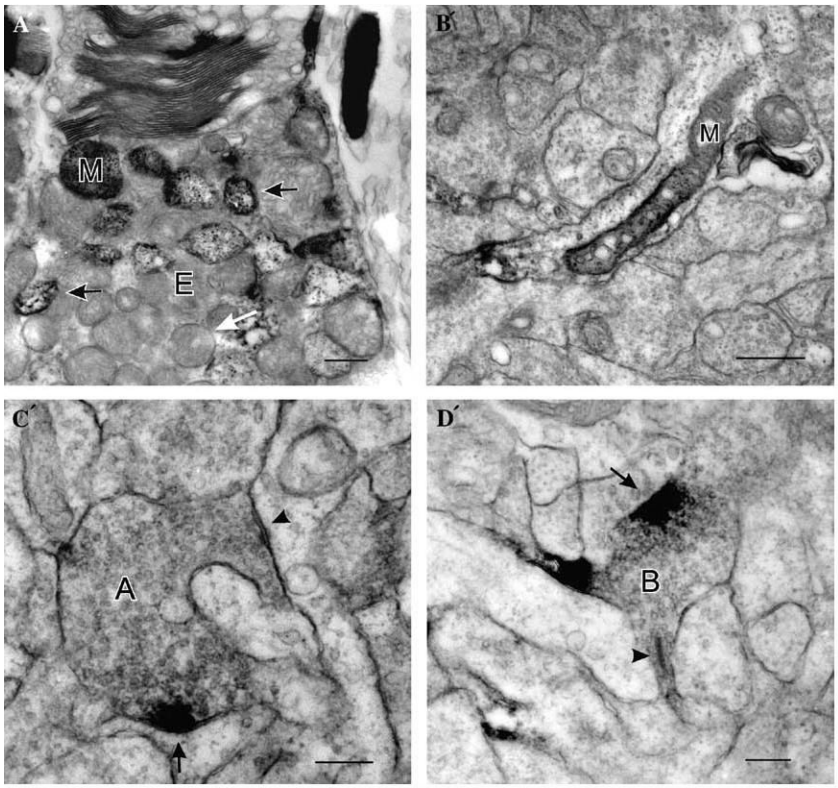

Fig. 3.

(A´) In some turtle photoreceptor ellipsoids (E) there were typical mitochondria (white arrow) and also some atypical mitochondria (black arrows) in the ellipsoids of rods and accessory elements of double cones (A) have nNOS-LI which increased their overall electron density and was most apparent in the intermembrane space. There was also some nNOS-LI associated with their outer segments. (B´) Some presumptive amacrine cell processes had mitochondria (M) with nNOS-LI. (C´) In some amacrine cell synaptic terminals, the nNOS-LI was only associated with the presynaptic region of conventional synapses (arrow in C´). Some amacrine cell synaptic terminals made more than one conventional synaptic contact, only some of which had nNOS-LI at their presynaptic specialization (C´, arrow, with nNOS-LI; arrowhead, without nNOS-LI). (D´) In some bipolar cell terminals (B), there was a patch of cytoplasmic nNOS-LI (arrow) associated with the plasma membrane some distance from the ribbon synapse (arrowhead). Scale bars: A´ and B´, 0.5 μm; C´ and D´, 0.25 μm.

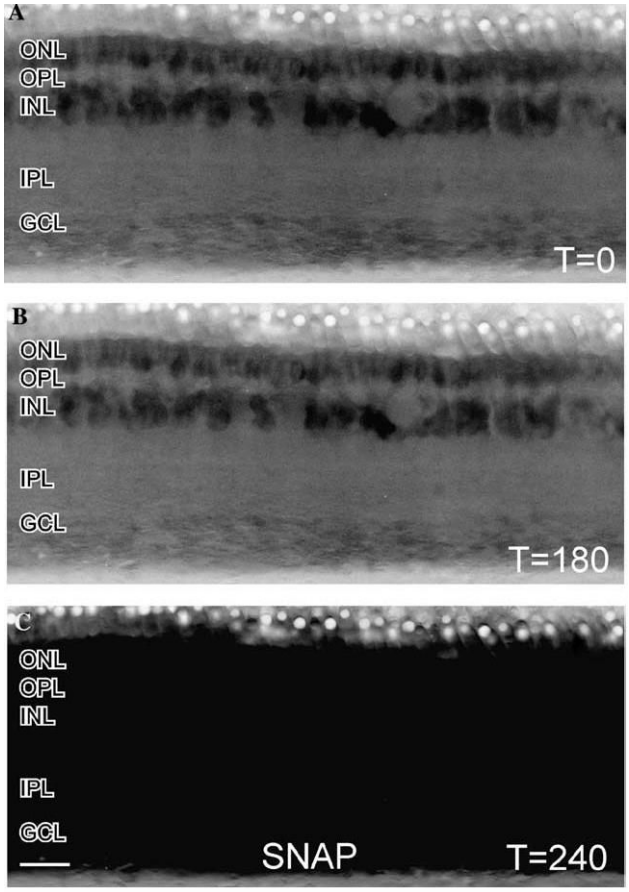

Fig. 4.

Effects of NO-donor on a turtle retinal slice loaded with DAF. (A) In these contt reversed images of a retinal slice loaded with DAF and illuminated with 488 nm light, there was some faint NO-IF apparent in the ONL and INL. (B) After 180 s of illumination there was only a slightly perceptible decrease in the levels of NO-IF which indicates that DAF is not activated by light alone. (C) Stimulation with 100 μM of the NO-donor SNAP at 180 s caused a dramatic and uniform increase in NO-IF throughout the slice by 240 s. This broad increase in NO-IF indicated that the entire slice was uniformly loaded with DAF. Scale bar, 20 μm

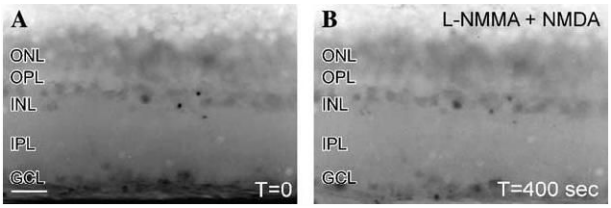

Fig. 5.

Effects of NOS inhibitor on the levels of NMDA stimulated increases in NO-IF. (A) A contrast reversed image of a DAF loaded retinal slice that was pre-incubated with the NOS inhibitor 100 μM LNMMA. In the absence of stimulation there was some faint NO-IF in some somata in the INL and GCL. (B) Even 400 s after stimulation with 250 lM NMDA there was still no increase in NO-IF which indicates that NMDA stimulated increases in NO-IF require the presence of enzymatically active NOS. Notice the decrease in endogenous NO-IF after 400 s of illumination. Scale bar, 20 lm.

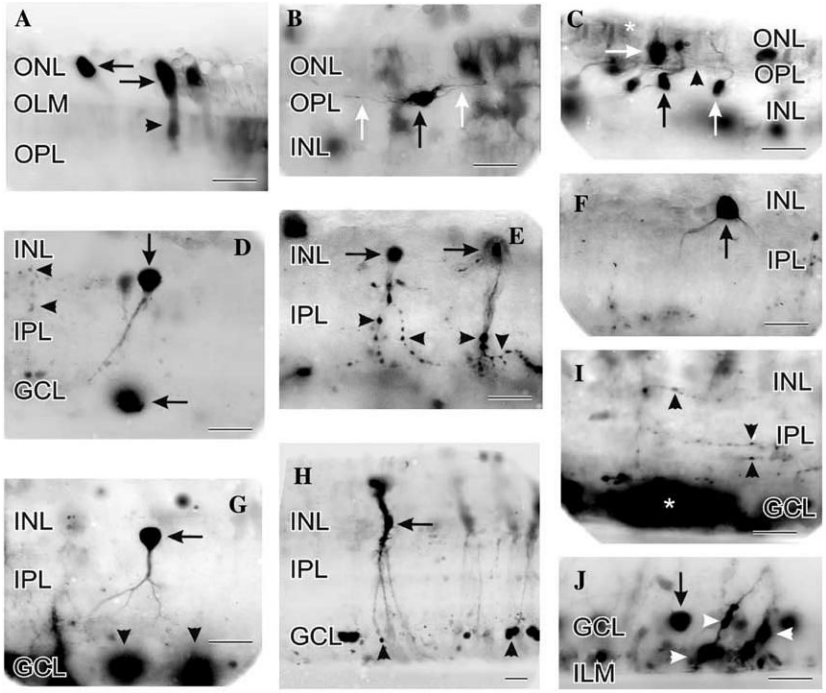

Fig. 6.

Contrast-reversed digital images of NMDA (100 lM) stimulated increases in NO-IF that was imaged real-time in living slices of turtle retina. (A) Strong NO-IF was concentrated in the ellipsoid region (horizontal arrows) of the inner segment of many photoreceptors. Lower levels of NO-IF were present in the somata and synaptic terminals of these cells (arrowhead). Diffuse weak NO-IF was also present at the OLM and OPL. (B) NO-IF was present in horizontal cell somata (black arrow) and their dendritic processes (white arrows) in the OPL. (C) Bipolar cell somata (both normally placed, vertical arrows; and displaced, horizontal arrow) and some of their processes in the OPL (arrowhead) exhibited NO-IF in response to NMDA. Diffuse NO-IF was also present in the ONL in the Landolts clubs of bipolar cells and in the apical processes of Müller cells (asterisk) near the OLM. (D) Amacrine cell soma (vertical arrow) with strong NO-IF in its soma and primary process. A soma in the GCL had strong NO-IF (horizontal arrow) that spread from the soma, while isolated boutons had smaller increases of NO-IF (horizontal arrowheads) that were more contained. (E) Amacrine cells (horizontal arrows) with strong NO-IF in their somata and in their process with many labeled boutons (arrowheads). Note that the NO-IF was quite strong and concentrated in the boutons. (F) Amacrine cell with strong NO-IF in its soma and primary processes that closely resembled a type 3 nNOS amacrine cell (vertical arrow). Although this cell type is the least common amacrine cell with nNOS-LI, they were frequently observed with NO-IF in response to NMDA. This suggested that these cells had a high density of NMDA receptors. (G) Amacrine cell (horizontal arrow) with strong NO-IF in its soma, and lower levels of NO-IF in its processes in the IPL. This cell does not clearly resemble previously described amacrine cell types with nNOS-LI. Several ganglion cell somata had strong NO-IF (arrowheads) which diffused into the surrounding GCL. (H) Müller cell with NO-IF in its soma (horizontal arrow) and processes. The NO-IF in Müller cells often began in small swellings on their processes (arrowheads) and spread up to fill their entire soma. (I) In response to NMDA, many amacrine cell processes and their associated boutons (vertical arrowheads) demonstrated NO-IF. The levels of NO-IF in the processes interconnecting the boutons were lower than in the boutons. In this slice, several somata in the GCL had very high levels of NO-IF that diffused to flood the entire GCL (asterisk). (J) In the region near the GCL and ILM, there were many somata (vertical arrow) and Müller cell

processes (horizontal arrow) with associated swellings (arrowheads) with elevated NO-IF. Scale bars, 20 lm.

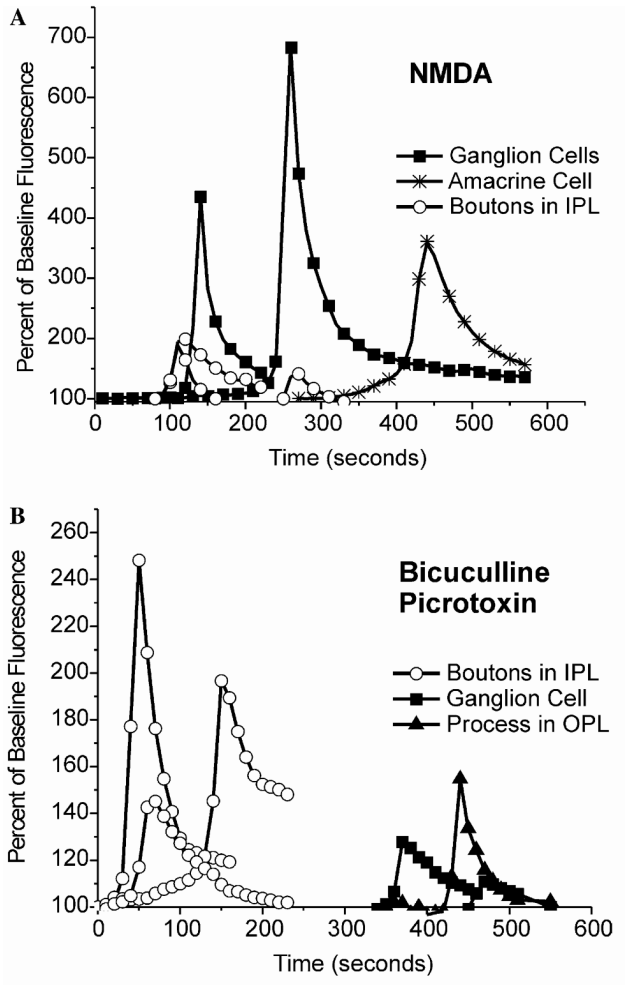

Fig. 7.

Quantitative analysis of increases in NO-IF in turtle in response to 100 μM NMDA (A) or a combination of 50 μM bicuculline and 50 lM picrotoxin (B). In all cases the drugs were added at time*T* = 0. Each of the curves represents the levels of NO-IF in relation to the unstimulated baseline fluorescence over time for a chosen region of interest of single example of the indicated structure. The overall levels of increases in NO-IF were greater for NMDA than for the combination of GABAergic antagonists. Each of the different cellular sources had characteristic time-courses for each pharmacological treatment even if there were differences in the overall intensity of the responses, i.e., ganglion cells (A) had similar kinetics. In some cases the production of NO-IF in boutons was much quicker in response to GABAergic antagonists than NMDA.

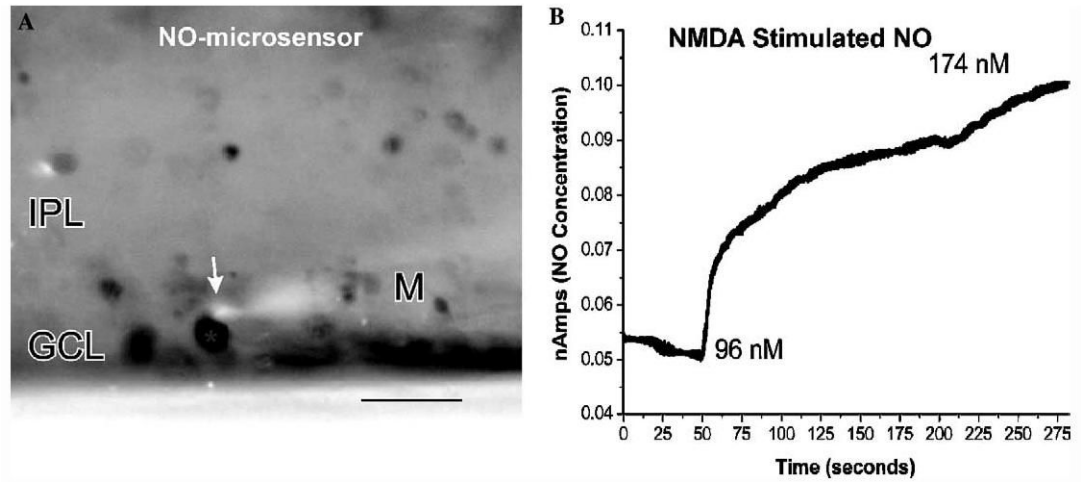

Fig. 8.

(A) Image of a NO selective microelectrode (M) with its sensor tip (arrow) placed adjacent to a ganglion cell with NO-IF in turtle. (B) Time-course of the increase in NO concentration measured with this microprobe. Before the application of NMDA the existing NO concentration in the region of this somata was ~96 nM, while after the NMDA stimulation the concentration rose to ~174 nM. Scale bar, 20 μm.

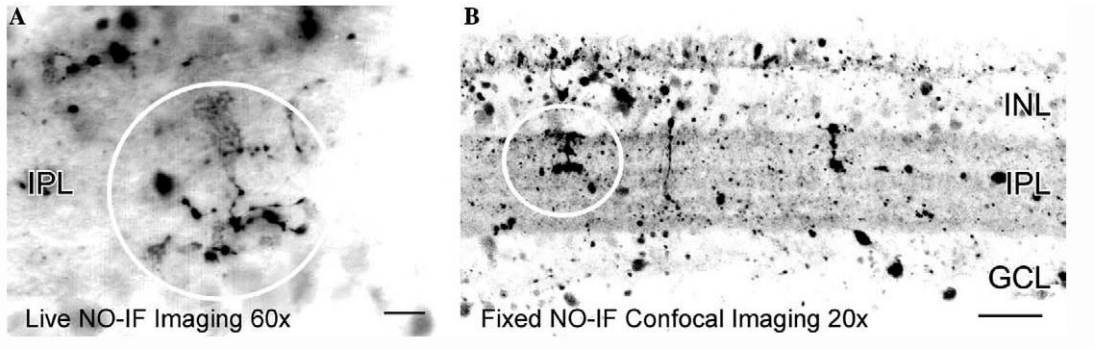

Fig. 9.

(A) Image of picrotoxin stimulated NO-IF in a slice of turtle retina. (B) A lower magnification image of NO-IF in a slice that was fixed with paraformaldehyde following stimulation with picrotoxin. The NO-IF seen in both the living and tissue is quite comparable. The circles in both A and B indicate comparable dendritic arborizations. Scale bars: A, 10 μm; B, 20 μm.

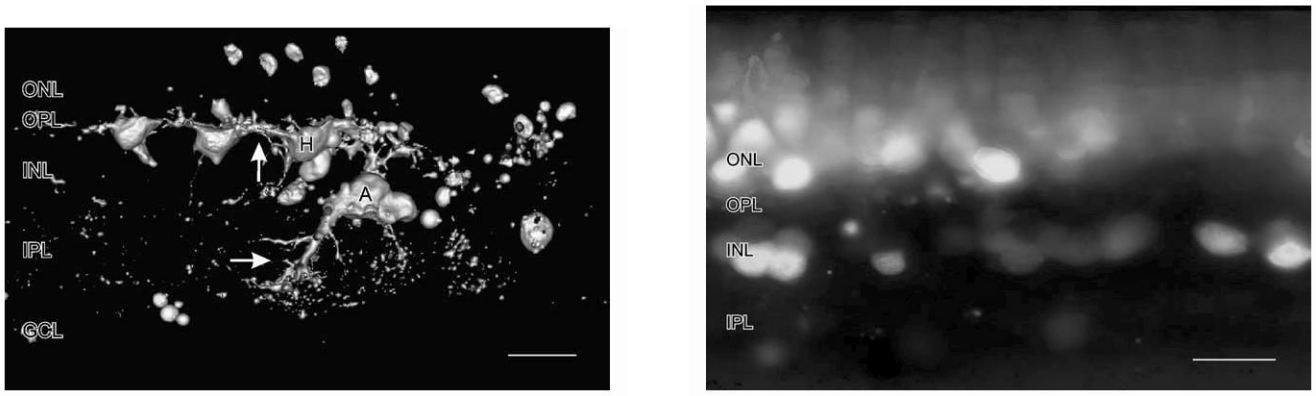

Fig. 10.

This is an image of NO-IF in a retinal slice made from a collapsed confocal stack that has been three-dimensionally rendered using the three-dimensional rendering software on a Zeiss LSM510NLO two-photon confocal microscope. This slice was stimulated using a 660-nm flashing light before being fixed with aldehydes. Note the excellent anatomical detail that is available of amacrine cells arborizations (A, horizontal arrow) and individual synaptic boutons in the IPL and horizontal cell arborizations in the OPL (H, vertical arrow). Scale bar, 20μm.

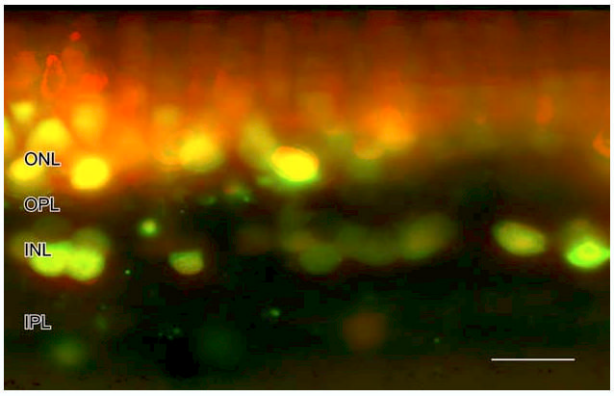

Fig. 11.

The red indicates the NO-IF that was present in salamander following 10 min of stimulation with 50 μm nicotine before fixation. The green indicates the NO-IF that was present following 30 min of paraformaldehyde fixation. The yellow indicates the NO-IF that was present before and after fixation. There is virtually no pure green in the image indicating that fixation did not induce or create any NO-IF that was not there prior to fixation. The red over the photoreceptors indicates that much of the NO-IF in the photoreceptors was lost during fixation. Scale bar, 20 lm.

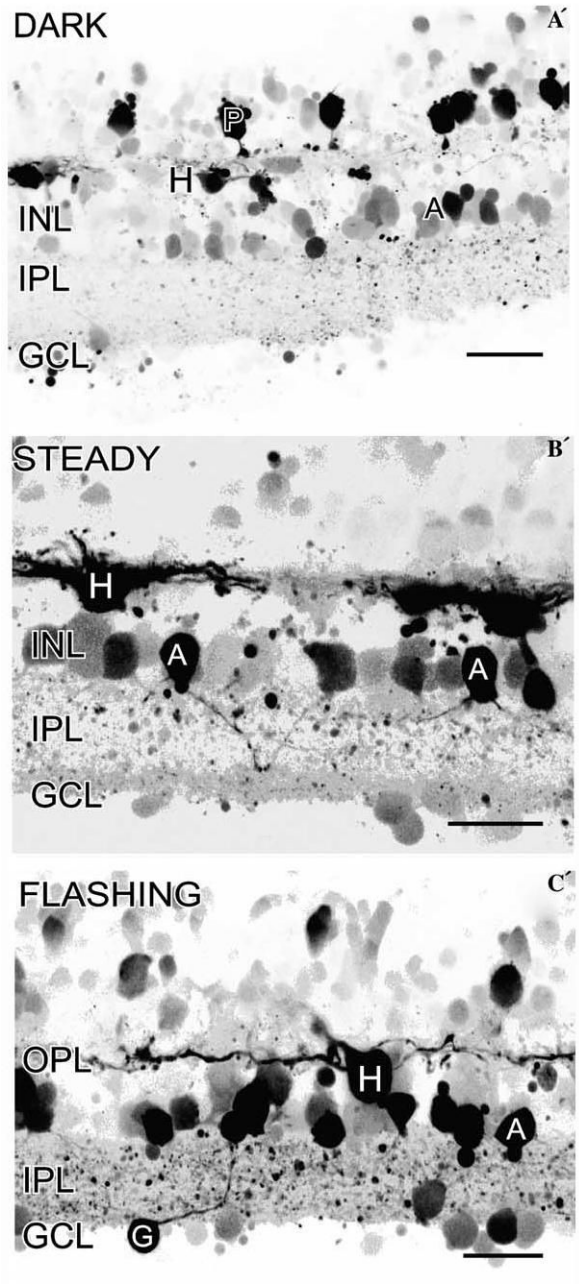

Fig. 12.

Imaging of NO-IF in response to different lighting conditions in salamander retina. (A´) In the dark, there was strong NO-IF in many horizontal cells (H), some photoreceptors (P), and some amacrine cell somata (A) in the INL. There may be a potential loss of NO-IF from photoreceptors so this labeling may be underrepresented. (B´) In steady light, there was still NO-IF in some photoreceptors and horizontal cells, but there were also some somata in the GCL and many amacrine cell somata (A) in the INL, and boutons in the IPL had strong NO-IF. (C´) In flashing light there was still strong NO-IF in the same sources seen with steady light, but there was strong NO-IF in more amacrine cell somata and their processes, in presumptive ganglion cell somata (G), and in numerous boutons in the IPL. Scale bars, 20 μm.

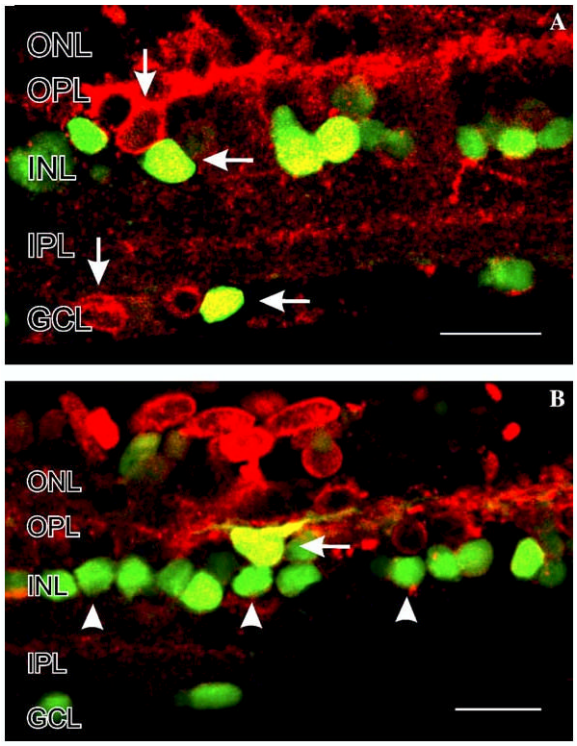

Fig. 13.

Colocalization of NO-IF and nNOS-LI in salamander retinal slices stimulated with 50 μM nicotine. In these images the NO-IF is green, the nNOS-LI is red, and yellow indicates that it was nNOS that was producing the NO-IF. The yellow double labeling indicates that nicotine primarily activates nNOS in somata in the INL and GCL (A and B, horizontal arrows). (A) In some horizontal cells in the INL and in some somata in the GCL, the nNOS is not activated by nicotine (vertical arrows). In some somata in the INL there is NO-IF but no nNOS-LI, which potentially indicates the activation of other isoforms of NOS than nNOS. Scale bars, 20 μm.

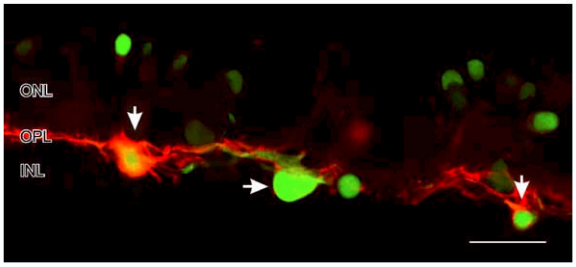

Fig. 14.

Colocalization of NO-IF and cGMP-LI in a salamander retinal slice stimulated with 50 μM nicotine. The NO-IF is green and the cGMP-LI is red. The horizontal cells on the left and right (vertical arrows) had both strong NO-IF and cGMP-LI, while the center horizontal cell (horizontal arrow) had primarily NO-IF. Note the apparent lack of NO-IF in the dendrites of these horizontal cells. Scale bar, 20 μm.